Assessment of kinetic models for the production of γ-valerolactone developed in isothermal, adiabatic and isoperibolic conditions

Wenel Naudy Vásquez Salcedo, Mélanie Mignot, Bruno Renou, Sébastien Leveneur

Assessment of kinetic models for the production of γ-valerolactone developed in isothermal, adiabatic and isoperibolic conditions

Wenel Naudy Vásquez Salcedo[1,2], Mélanie Mignot[3], Bruno Renou[2], Sébastien Leveneur[1*]

[1]*INSA Rouen Normandie, UNIROUEN, Normandie Univ, LSPC, UR4704, F-76000 Rouen, France, France, Corresponding author (*):* sebastien.leveneur@insa-rouen.fr

[2]*Normandie Univ., UNIROUEN, INSA Rouen, CNRS, CORIA, 76000 Rouen, France*

[3]*Normandie Université, INSA Rouen, UNIROUEN, CNRS, COBRA Laboratory, F-76000 Rouen, France*

Abstract

The use of lignocellulosic biomass as raw materials for the production of biofuels is increasing. There are several potential processes valorizing these raw materials, but the shift from lab-scale to industrial scale requires the development of reliable and robust kinetic models. Usually, these models are developed in isothermal mode, limiting their use for thermal risk assessment or pinch analysis. We developed and assessed several kinetic models for the hydrogenation of butyl levulinate to γ-valerolactone over Ru/C in different thermal modes, i.e., isothermal, isoperibolic and adiabatic modes. The reaction calorimeter Mettler-Toledo RC1 was used to perform kinetic experiments. Bayesian inference was used during the regression stage to calculate the credible intervals. The validation stage was done by a holdout method. From the regression and validation stage, we found that the non-competitive Langmuir Hinshelwood with hydrogen non-dissociation and dissociation were the most reliable models. These models can predict the kinetics of this reaction system in different thermal modes.

Keywords: kinetic modeling, gamma valerolactone, levulinate, calorimetry, adiabatic

Abbreviations

Cp	Specific heat capacity [$J.kg^{-1}.K^{-1}$]
Ea	Activation energy [$J.mol^{-1}$]
$f_{iu}(\xi)$	Estimated concentration or temperature
He	Henry's coefficient [$mol.m^{-3}.bar^{-1}$]
k	Rate constant
K*i*	Adsorption rate of specie *i* [$m^3.mol^{-1}$]
$k_L.a$	Volumetric mass transfer coefficient [s^{-1}]
$(k_L.a)_{modified}$	Modified volumetric mass transfer coefficient [$(Pa{\cdot}s{\cdot}K^{-1})^{0.5}(Pa{\cdot}s{\cdot}kg^{-1}{\cdot}m^{-3})^{0.25}{\cdot}s^{-1}$]
m	Mass [kg]
P	Pressure [bar]
R_i	Reaction rate *i* [$mol.m^{-3}.s^{-1}$]
R	Gas constant [$J.mol^{-1}.K^{-1}$]
T	Temperature [K]
UA	Global heat transfer coefficient [$W.K^{-1}$]
$\lvert v(\xi)\rvert$	Determinant of the covariance matrix of responses
Y_i	Experimental concentration of specie i or temperature

Greek letters

$\omega_{Cat.}$	Catalyst loading [$kg.m^{-3}$]
μ_{liq}	Liquid viscosity [Pa·s]
ρ_{liq}	Mass density [$kg{\cdot}m^{-3}$]

32 Subscripts and superscripts

Liq	Liquid phase
Ref	Reference
o	Initial
*	Interfacial value

33

34 Abbreviations

AIC	Akaike information criterion
BL	Butyl levulinate
BHP	Butyl 4-hydroxypentanoate
BuOH	Butanol
ER	Eley-Rideal kinetic model with no adsorption of hydrogen
GC	Gas chromatography
GVL	γ-valerolactone
HPD	Highest Posterior Density
LH1	Langmuir-Hinshelwood kinetic model with molecular adsorption of hydrogen
LH2	Langmuir-Hinshelwood kinetic model with hydrogen dissociation
NCLH1	Non-competitive Langmuir-Hinshelwood kinetic model with no dissociation of hydrogen
NCLH2	Non-competitive Langmuir-Hinshelwood kinetic model with hydrogen dissociation
ODEs	Ordinary differential equation system
OF(ξ)	Objective function
RKMC	Redlich-Kwong-Mathias-Copeman equation of state
Ru/C	Ruthenium on activated carbon

35

1. Introduction

Our dependency on fossil raw materials is very high in the modern society. Over 80% of the world's primary energy consumption in the energy sector was from fossil raw materials in 2020 [1].

The use of lignocellulosic biomass (LCB) for biofuel production is seen as a better alternative to fossil fuel because of its global availability, lower environmental impact, and cost [2–6]. Besides, such raw materials are not in competition with the alimentary sector, avoiding the dilemma of food versus fuel [7,8]. The sugar parts of LCB, i.e., cellulose and hemicellulose, are mainly used to produce chemicals, materials or fuels. The valorization of these polymers of sugar can lead to several platform molecules and their derivatives, such as succinic acid, furfural, 5-HMF, levulinic acid, glycerol, etc. [9–12].

The chemical γ-valerolactone (GVL), produced from the hydrogenation of levulinic acid or ester levulinate, is also considered as a platform molecule [13,14]. Hydrogenation of bio-based carboxylic acids, esters or related compounds is considered a step toward a sustainable and carbon-neutral process [15]. In fine chemistry, GVL is considered an excellent aprotic solvent [16–21] because of its low vapor pressure, high flash point, and potential to increase acid activity [22–26]. In polymer science, GVL is a promising starting material for producing greener monomers [27–30].

In the energy field, GVL cannot be used directly as a fuel [31], but it can be used as an additive fuel [32–35]. GVL is a promising feedstock for producing hydrocarbon fuels [31,36–42] or pentanoic biofuels [43].

From a safety, cost and environmental standpoint, determining the best operating conditions for the production of GVL is vital [44–46]. The literature proposes several routes for producing GVL by hydrogenating raw lignocellulosic biomass, cellulose, glucose or fructose [47]. These different routes require the hydrogenation of levulinic acid or alkyl levulinates, and there are three different hydrogenation options:

-use of molecular hydrogen [34,48–65]

-*in situ* FA decomposition producing hydrogen [66–74]

-Meerwein-Ponndorf-Verley reaction involving the use of alcohol for hydrogen transfer [75–82]

The use of molecular hydrogen and ruthenium-based catalyst is the most efficient system to produce GVL. Developing such a process at an industrial scale requires reliable and robust kinetic models. Such models are essential to optimize the operating cost to get the highest GVL yield. There are several models for the hydrogenation of levulinates or levulinic acid [52,53,57,64,83–87]. These models were developed using experiments performed in isothermal mode, and could limit their application to pinch analysis or process safety.

Generally speaking, the development of kinetic models in different thermal modes, e.g., isothermal, adiabatic, isoperibolic, or dynamic modes, is quite seldom in the literature.

In adiabatic mode, one can only use the reaction temperature as an observable [88–90] allowing to obtain reliable models for thermal risk assessment [91]. It is impossible to withdraw samples during the reaction; otherwise, the reaction temperature signal is perturbed. Hence, kinetic models only developed in adiabatic mode are limited for thermal risk assessment.

In isoperibolic mode, for some chemical systems, it is possible to track the reaction temperature and withdraw some samples to track the concentration in the liquid phase [92–94], allowing the development of reliable kinetic models considering concentration and temperature as observables.

There is a need to have kinetic models developed in different thermal modes to improve their reliability and robustness and to be used universally for process safety, process intensification, and cost evaluation. To do that, one must carry out different experiments in isothermal conditions to track the species concentration and in non-isothermal conditions (isoperibolic and adiabatic modes) to track the reaction temperature.

To the best of the authors' knowledge, such an approach is highly seldom in the literature [94]. In this study, we developed kinetic models for the hydrogenation of butyl levulinate into GVL over Ru/C in three thermal modes: isothermal, isoperibolic and adiabatic. A high concentrated solution of BL was used to perform experiments. The state-of-the-art reaction calorimeter Mettler-Toledo RC1 was used to perform experiments in different thermal modes. The developed models were validated to assess their

87 reliability and select the most reliable ones. Butyl levulinate was chosen because it is gaining a lot of
88 interest as a platform molecule and can be used in different areas [16,95].
89

2. Experimental section

2.1. Chemicals

Chemicals used during this research for analytical and experimental purposes were purchased from different providers and used without further purification: n-Butyl levulinate (n-BL), acquired from Alfa Aesar with a purity ≥ 98%, CAS: 2052-15-5. Hydrogen gas (H_2), acquired from Linde group with a purity ≥ 99.99%, CAS: 1333-74-0. γ-Valerolactone (GVL), acquired from Sigma Aldrich with a purity ≥ 99%, CAS: 108-29-2. 1-Butanol (BuOH), acquired from LabLine with a purity ≥ 99%, CAS: 71-36-3. Ruthenium on activated carbon (Ru/C), acquired from Alfa Aesar, 5% of ruthenium powder, reduced, 50% nominally wet, CAS: 7440-18-8. Acetone, acquired from Fischer Scientific with a purity ≥ 99%, CAS: 67-64-1.

2.2. Analytical system

Gas chromatography coupled with a flame ionization detector (GC-FID) technique was applied to quantify the amount of chemicals in samples. GC-FID equipment is from Scion Instruments supplier. GC-FID was equipped with a low polarity column (Phenomenex, ZB-5) composed of 95% dimethyl siloxane and 5% of phenyl groups. Column dimensions: length: 30 m, internal diameter: 0.32 mm, coating width: 0.25 µm.

Helium (99.99%) was used as carrier gas at a constant flow rate of 1.2 mL/min. The temperature of the injector and the detector were set at 250 °C. The oven temperature ramp was set to 50 °C (1 min) – 20 °C /min – 200 °C (1 min). Samples were diluted in acetone to be analyzed, the injection volume was 1 µL and the split ratio was 20:1.

2.3. RC1 reactor

To develop a robust kinetic model for GVL production from n-BL, different experiments were performed in the Mettler-Toledo RC1mx calorimeter, considering isothermal and non-isothermal conditions.

The RC1mx is a high-performance calorimeter with a heating and cooling loop system, allowing us to have a very accurate temperature control of the reaction media. The RC1mx vessel is made of Hastelloy C22 metal one, with a 1.8 L capacity and 100 bar of tolerance. A gas inlet and outlet system are connected to the vessel to control the pressure. A PID automatically controls this system. The RC1mx is also equipped with a calibration heater that evaluates the heat capacity (Cp) and the reaction media's global heat transfer coefficient (UA). Fig. 1 represents the RC1mx installation.

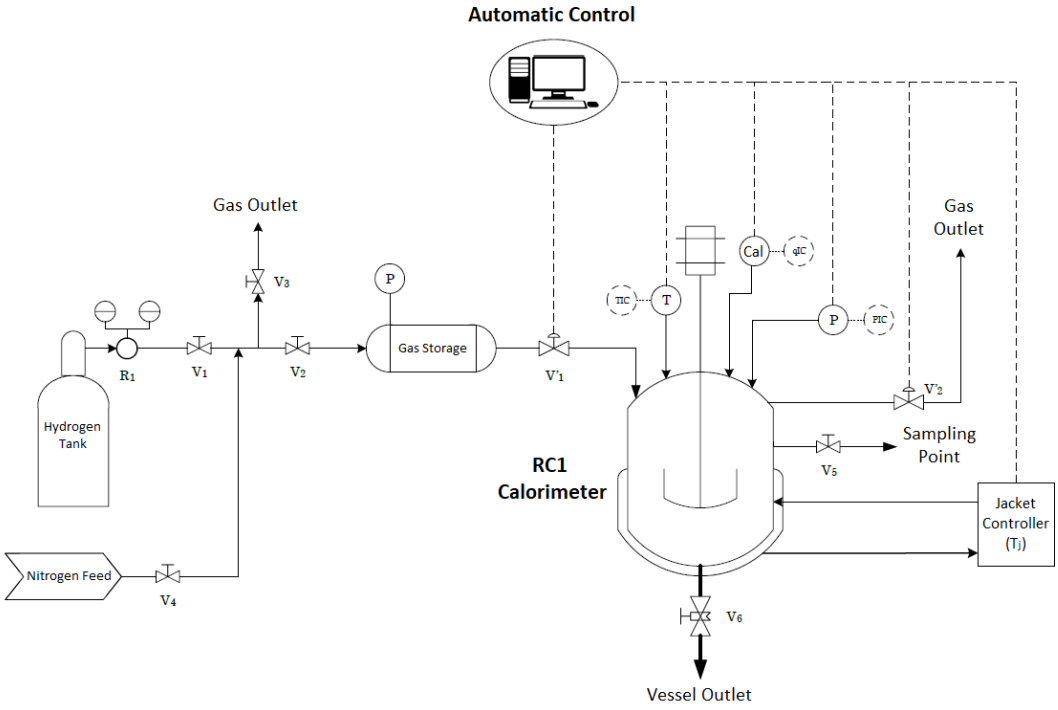

Fig. 1. RC1mx Calorimeter installation.

2.4. Determination of the global heat transfer

The global heat transfer UA plays a fundamental role in the energy balance to characterize the transfer between the heat carrier and reaction temperature. Thus, it is vital to measure it correctly. This value was determined by electrical calibration [96–98]. Calibration experiments were performed without catalysts, and a highly concentrated solution of BL, i.e., weight percentage higher than 98%, was used initially. We varied the temperature and rotating speed to be able to draw the Wilson plot.

2.5. Gas-liquid mass transfer measurement

Table 1 shows the experimental matrix for mass transfer study. These experiments were performed in the absence of catalyst to avoid chemical reactions. The Redlich–Kwong–Mathias–Copeman (RKMC) equation of state was used to quantify the number of moles of hydrogen into the gas phase. According to Nasrifar, the RKMC equation is more accurate and robust [99].

Table 1. Experimental matrix for gas-liquid mass transfer measurement.

Run	m_0BL (kg)	Tr_0 (K)	P (bar)
1_MT	0.520	373.15	25
2_MT	0.520	373.15	25
3_MT	0.520	413.15	25
4_MT	0.520	433.15	25

2.6. Kinetic modeling

Parameter estimation, simulation and curve fitting were performed using the commercial software Athena Visual Studio V.14.2 [100]. Athena Visual Studio uses a Bayesian framework more suitable for multi-response parameter estimation than the classical nonlinear least squares method [101,102]. Indeed, Bayesian inference requires calculating the determinant criterion [103].

The following observables were used for the parameter estimation stage: BL, BHP, GVL and reaction temperatures. Only two samples were withdrawn for experiments performed in isoperibolic or adiabatic conditions: at the beginning and the end of the reaction. Several samples were withdrawn for isothermal kinetic experiments, and the reaction temperature was constant.

The ODEs, obtained from material and energy balances, were integrated by the DDAPLUS solver, a modified Newton algorithm [104]. The GREGPLUS subroutine package was used to minimize the objective function OF(ζ) and to calculate the highest probability density HPD, i.e., credible intervals, of the estimated parameters and the normalized covariance matrix.

GREGPLUS uses successive quadratic programming starting from our initial guess values to minimize OF(ζ) [100].

$$OF(\xi) = (a + b + 1) \cdot ln|v(\xi)| \quad (1)$$

where a is the number of events in response, b is the number of responses and $|v(\xi)|$ is the determinant of the covariance matrix of the responses.

Each element of the covariance matrix of the responses is

$$v_{ij}(\xi) = \sum_{u=1}^{n} \omega_u \cdot [Y_{iu} - f_{iu}(\xi)] \cdot \left[Y_{ju} - f_{ju}(\xi)\right] \quad (2)$$

where, ω_u is the weight factor, Y_{iu} the experimental concentration or temperature and $f_{iu}(\xi)$ the estimated value for response *i* and event *u*; Y_{ju} the experimental concentration and $f_{ju}(\xi)$ the estimated value for response *j* and event *u*.

A modified Arrhenius equation was used to decrease the correlation between the pre-exponential factor and the activation energy by linearizing the original Arrhenius equation as

$$k(T) = exp\left[ln\left(k\left(T_{ref}\right)\right) + \frac{E_a}{R \cdot T_{ref}} \cdot \left(1 - \frac{T_{ref}}{T}\right)\right] \quad (3)$$

where, T_{ref} is the reference temperature chosen in the considered experimental temperature range. Table 2 shows the experimental matrix for the regression and Table 3 shows the experimental matrix for the validation stage.

Table 2. Experimental matrix for regression with initial conditions.

Run	P (bar)	m_0BL (kg)	m_0GVL (kg)	m_0Ru (kg)	Cp_0 ($J \cdot kg^{-1} \cdot K^{-1}$)	UA_0 ($W \cdot K^{-1}$)	$[BL]_0$ ($mol \cdot m^{-3}$)	$[BHP]_0$ ($mol \cdot m^{-3}$)	$[GVL]_0$ ($mol \cdot m^{-3}$)	$[BuOH]_0$ ($mol \cdot m^{-3}$)	Tr_0 (K)	Thermal mode
1	35	0.415	0.105	0.005	2736	17	4712	0	2082	29	393	isothermal
2	35	0.500	0.000	0.007	2736	19	5929	0	28	65	423	isothermal
3	35	0.500	0.000	0.007	2736	19	9	2222	3909	2883	432	isothermal
4	15	0.117	0.402	0.004	2736	17	1359	2	8198	8	403	isothermal
5	20	0.520	0.000	0.006	3131	17	6105	0	4	3	394	isothermal
1	22	0.500	0.000	0.005	2755	18	6114	0	0	0	412	isoperibolic
2	30	0.400	0.100	0.005	2773	17	4963	0	2079	0	392	isoperibolic
3	30	0.420	0.100	0.005	2646	17	4713	1	1853	31	403	isoperibolic
4	35	0.420	0.100	0.008	3131	17	5090	1	2040	3	393	isoperibolic
1	36	0.520	0.000	0.006	2751	17	5816	0	0	0	393	adiabatic
2	35	0.520	0.000	0.006	2789	15	6056	0	3	53	373	adiabatic
3	25	0.520	0.000	0.005	2704	15	5360	0	0	0	373	adiabatic
4	35	0.420	0.100	0.007	2624	15	4553	0	1786	31	373	adiabatic
5	25	0.520	0.000	0.006	2705	16	5635	0	20	37	383	adiabatic
6	30	0.350	0.170	0.008	2705	17	4223	4	3384	25	403	adiabatic
7	25	0.400	0.120	0.005	3131	18	4681	10	2337	30	413	adiabatic
8	20	0.520	0.000	0.004	3131	17	6339	0	8	62	403	adiabatic

174 Table 3. Experimental matrix with initial conditions for validation

Run	P (bar)	m_0BL (kg)	m_0GVL (kg)	m_0Ru (kg)	Cp_0 ($J \cdot kg^{-1} \cdot K^{-1}$)	UA_0 ($W \cdot K^{-1}$)	$[BL]_0$ ($mol \cdot m^{-3}$)	$[BHP]_0$ ($mol \cdot m^{-3}$)	$[GVL]_0$ ($mol \cdot m^{-3}$)	$[BuOH]_0$ ($mol \cdot m^{-3}$)	Tr_0 (K)	Thermal mode
6	38	0.415	0.105	0.005	2736	17	1050	2202	3482	1356	403	isothermal
7	35	0.415	0.105	0.005	2736	15	5059	0	2092	0	373	isothermal
8	20	0.520	0.000	0.006	2736	16	5756	0	4	34	384	isothermal
5	35	0.520	0.000	0.007	2788	15	5857	0	0	0	373	isoperibolic
6	35	0.420	0.100	0.008	2728	16	4984	1	1993	33	383	isoperibolic

175

3. Results and discussion

3.1. Kinetics

The global kinetics for the hydrogenation of BL is a two-step reaction (Fig. 2).

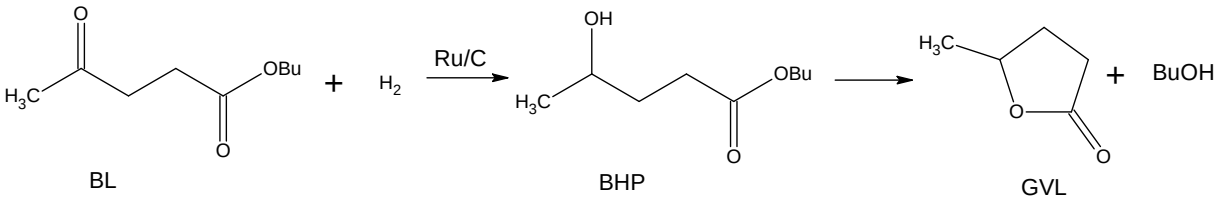

Fig. 2. Reaction pathway for the hydrogenation of BL over Ru/C.

The hydrogenation of the carbonyl group can take different routes, as illustrated in a previous article of our group [105]. In this work we considered five kinetic models to determine the most reliable, these kinetic models are described below:

- Eley-Rideal (ER1): This kinetic model considers that only BL is adsorbed into active sites of the catalyst, and then molecular hydrogen collides directly to the adsorbed BL.
- Langmuir Hinshelwood with molecular adsorption of H_2 (LH1): This kinetic model considers that all reactants, BL and molecular hydrogen, are adsorbed into the active sites of the catalyst without dissociation, then the chemical reaction takes place between adsorbed molecules.
- Langmuir Hinshelwood with hydrogen dissociation (LH2): As LH1 this kinetic model considers that all reactants, BL and molecular hydrogen, are adsorbed into the active sites of the catalyst. However, in this case, molecular hydrogen is dissociated into atomic hydrogen; then the chemical reaction takes place between adsorbed BL and adsorbed atomic hydrogen.
- Non-competitive Langmuir Hinshelwood with molecular adsorption of H_2 (NCLH1): This kinetic model considers that there is no competition between the reactants for the active sites of the catalyst, so that it is considered that BL and molecular hydrogen are adsorbed in different actives sites. Chemical reaction occurs between adsorbed BL and adsorbed molecular hydrogen without dissociation.
- Non-competitive Langmuir Hinshelwood with hydrogen dissociation (NCLH2): As NCLH1 this kinetic model consider that there is no competition between the reactants. BL and molecular

hydrogen are adsorbed into different actives sites, then the adsorbed molecular hydrogen is dissociated into atomic hydrogen. The chemical reaction occurs between adsorbed BL and adsorbed atomic hydrogen.

Table 4 shows the rate expression for the different possible reaction mechanisms.

Table 4. Kinetic expression for the different mechanisms for the hydrogenation step.

Kinetic model	Rate expression
Eley-Rideal with no adsorption of hydrogen (ER1)	$\frac{k_1 \cdot [H_2] \cdot K_{BL} \cdot [BL] \cdot \omega_{Cat.}}{(K_{BL} \cdot [BL] + K_{BHP} \cdot [BHP] + 1)}$
Langmuir Hinshelwood with molecular adsorption of H_2 (LH1)	$\frac{k_1 \cdot K_{H2} \cdot [H_2] \cdot K_{BL} \cdot [BL] \cdot \omega_{Cat.}}{(K_{H2} \cdot [H_2] + K_{BL} \cdot [BL] + K_{BHP} \cdot [BHP] + 1)^2}$
Langmuir Hinshelwood with hydrogen dissociation (LH2)	$\frac{k_1 \cdot K_H \cdot [H_2] \cdot K_i \cdot K_{BL} \cdot [BL] \cdot \omega_{Cat.}}{\left(\sqrt{K_H \cdot [H_2]} + K_{BL} \cdot [BL] + K_{BHP} \cdot [BHP] + K_i \cdot K_{BL} \cdot [BL] \cdot \sqrt{K_H \cdot [H_2]} + 1\right)^2}$
Non-competitive Langmuir Hinshelwood with no dissociation of hydrogen (NCLH1)	$\frac{k_1 \cdot K_{H2} \cdot [H_2]}{(1 + K_{H2} \cdot [H_2])} \cdot \frac{K_{BL^\wedge} \cdot [BL]}{(1 + K_{BHP^\wedge} \cdot [BHP] + K_{BL^\wedge} \cdot [BL])} \cdot \omega_{Cat.}$
Non-competitive Langmuir Hinshelwood with hydrogen dissociation (NCLH2)	$\frac{k_1 \cdot K_H \cdot K_C \cdot K_{BL^\wedge} \cdot [H_2]}{\sqrt{K_H \cdot [H_2]} + 1} \cdot \frac{[BL] \cdot \omega_{Cat.}}{K_{BL^\wedge} \cdot [BL] + K_C \cdot \sqrt{K_H \cdot [H_2]} \cdot K_{BL^\wedge} \cdot [BL] + K_{BHP^\wedge} \cdot [BHP] + 1}$

The kinetic expression for the second reaction step, i.e., the cyclization step, was expressed as

$$R_{Cyclization} = k_2 \cdot [BHP] \quad (4)$$

We applied linearization on the rate constant, and kinetic factors are displayed in Table 5.

212 Table 5. Kinetic factors and estimated parameters.

Models	Kinetic factors	Estimated parameters
ER1	$exp\left(ln(K_{BL}) + ln\left(k_1(T_{ref})\right) + \frac{E_{a1}}{R \cdot T_{ref}} \cdot \left(1 - \frac{T_{ref}}{T}\right)\right)$	$ln(K_{BL})$, $ln\left(k_1(T_{ref})\right)$, $\frac{E_{a1}}{R \cdot T_{ref}}$ and $ln(K_{BHP})$
LH1	$exp\left(ln(K_{H2}) + ln(K_{BL}) + ln\left(k_1(T_{ref})\right) + \frac{E_{a1}}{R \cdot T_{ref}} \cdot \left(1 - \frac{T_{ref}}{T}\right)\right)$	$ln(K_{H2})$, $ln(K_{BL})$, $ln\left(k_1(T_{ref})\right)$, $\frac{E_{a1}}{R \cdot T_{ref}}$ and $ln(K_{BHP})$
LH2	$exp\left(ln(K_H) + ln(K_{BL}) + ln(K_i) + ln\left(k_1(T_{ref})\right) + \frac{E_{a1}}{R \cdot T_{ref}} \cdot \left(1 - \frac{T_{ref}}{T}\right)\right)$	$ln(K_H)$, $ln(K_{BL})$, $ln(K_i)$, $ln\left(k_1(T_{ref})\right)$, $\frac{E_{a1}}{R \cdot T_{ref}}$ and $ln(K_{BHP})$
NCLH1	$exp\left(ln(K_{H2}) + ln(K_{BL^\wedge}) + ln\left(k_1(T_{ref})\right) + \frac{E_{a1}}{R \cdot T_{ref}} \cdot \left(1 - \frac{T_{ref}}{T}\right)\right)$	$ln(K_{H2})$, $ln(K_{BL^\wedge})$, $ln(K_{BHP^\wedge})$, $ln\left(k_1(T_{ref})\right)$ and $\frac{E_{a1}}{R \cdot T_{ref}}$
NCLH2	$exp\left(ln(K_H) + ln(K_{BL^\wedge}) + ln(K_C) + ln\left(k_1(T_{ref})\right) + \frac{E_{a1}}{R \cdot T_{ref}} \cdot \left(1 - \frac{T_{ref}}{T}\right)\right)$	$ln(K_H)$, $ln(K_{BL^\wedge})$, $ln(K_{BHP^\wedge})$, $ln(K_c)$, $ln\left(k_1(T_{ref})\right)$ and $\frac{E_{a1}}{R \cdot T_{ref}}$

213

3.2. Material and energy balances

Due to the vigorous stirring, ideal hydrodynamics was assumed in the RC1 reactor. Material balances for different compounds in the liquid phase leads to:

$$\frac{dC_{BL}}{dt} = -R_{Hydrogenation} \quad (5)$$

$$\frac{d[H_2]_{liq}}{dt} = k_L.a \cdot \left([H_2]^*_{liq} - [H_2]_{liq}\right) - R_{Hydrogenation} \quad (6)$$

$$\frac{dC_{BHP}}{dt} = R_{Hydrogenation} - R_{Cyclization} \quad (7)$$

$$\frac{dC_{BuOH}}{dt} = R_{Cyclization} \quad (8)$$

$$\frac{dC_{GVL}}{dt} = R_{Cyclization} \quad (9)$$

The term $[H_2]^*_{liq}$ is hydrogen concentration at the gas-liquid interface. This value depends on temperature and was determined through Henry's constant: $He(T) = \frac{[H_2]^*_{liq}}{P_{H_2,Reactor}}$ [54]. A separate mass transfer coefficient study was carried out to estimate the volumetric gas-to-liquid mass transfer coefficient for hydrogen. A similar methodology applied in a previous study of our group was used [57] to estimate this mass transfer coefficient by taking into account density and viscosity of the reaction mixture [106]. For the sake of clarity, this information was added in Supplementary Material (S1). The value of $He(T)$ can change with temperature and chemical composition, the results from Capecci et al. were used [54].

The heat balance equation for the liquid phase leads to

$$\frac{\mathrm{d}T_R}{dt} = \frac{\left(-R_{Hydrogenation}\cdot\Delta H_{R,Hydrogenation}\cdot V - R_{Cyclization}\cdot\Delta H_{R,Cyclization}\cdot V\right) + UA\cdot\left(T_j - T_R\right) + \alpha\cdot\left(T_{amb} - T_R\right)}{m_R\cdot C_{PR} + m_{insert}\cdot Cp_{insert} + m_{catalyst}\cdot Cp_{catalyst}} \quad (10)$$

The term $\alpha \cdot (T_{amb} - T_R)$ represents the heat loss with the surroundings. The term $UA \cdot \left(T_j - T_R\right)$ is the heat flow rate exchanged with the heat carrier, and UA is the global heat transfer, T_j and T_R are the jacket and reaction temperatures. The term $m_R \cdot C_{PR} + m_{insert} \cdot Cp_{insert} + m_{catalyst} \cdot Cp_{catalyst}$ represents the

thermal inertia, where $m_{insert} \cdot Cp_{insert}$ is equal to 52 $J \cdot K^{-1}$, according to the manufacturer, C_{PR} was evaluated based on the evolution of chemical composition and temperature [24] and $Cp_{catalyst}$ was found based on the article of Lu et al. [107]. Reaction enthalpies for hydrogenation $\Delta H_{R,Hydrogenation}$ and cyclization $\Delta H_{R,Cyclization}$ were the ones calculated by Wang et al. [46].

3.3. Calibration results (Wilson plot)

In order to verify the thin wall approximation between the heat carrier and reaction mixture and to predict the UA values with reaction temperature, UA value was calculated at different temperatures and rotating speeds in the absence of reaction, i.e., Wilson plot [98]. Fig. 3 shows the linearity between 1/UA and $N^{-2/3}$, confirming the thin wall approximation.

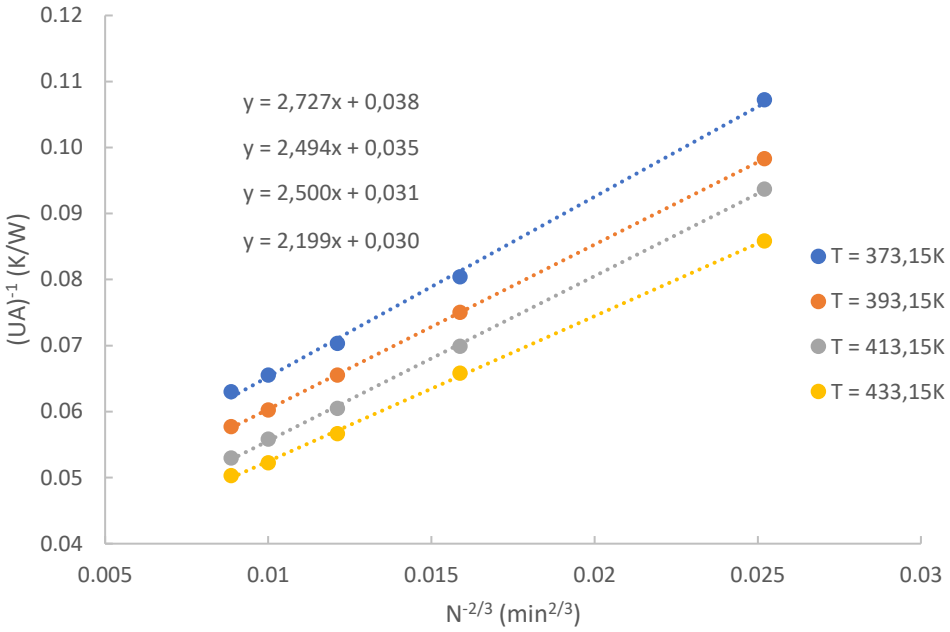

Fig. 3. Wilson plot.

3.4. Gas-liquid mass transfer results

In these experiments, rates of hydrogenation and cyclization are equal to zero, thus one should integrate Eq. (6) to estimate the $k_L a$ value. The volumetric mass transfer coefficient was expressed as [57]:

$$k_L a = (k_L a)_{modified} \cdot \left(\frac{T_{liq}}{\mu_{liq}}\right)^{0.5} \cdot \left(\frac{\rho_{liq}}{\mu_{liq}}\right)^{0.25} \quad (11)$$

The constant $(k_L a)_{modified}$ was calculated from experiments shown in Table 1 as described in Supplementary Material (S1). From Table S1.1, one can notice that the calculated value of $(k_L a)_{modified}$ for each run is very similar. The average value of $(k_L a)_{modified}$ was found to be $2.25 \cdot 10^{-6}$ $(Pa \cdot s \cdot K^{-1})^{0.5}(Pa \cdot s \cdot kg^{-1} \cdot m^{-3})^{0.25} \cdot s^{-1}$ and the standard deviation was equal to 0.14 $(Pa \cdot s \cdot K^{-1})^{0.5}(Pa \cdot s \cdot kg^{-1} \cdot m^{-3})^{0.25} \cdot s^{-1}$. This value was found to be similar than the one of Wang et al. [57].

3.5. Kinetic modeling

3.5.1. Regression

The five models were tested during the regression (ER1, LH1, LH2, NCLH1 and NCLH2). The Akaike information criterion (AIC) was used to evaluate the most reliable models, and it was calculated as

$$AIC: number\ of\ independant\ event \cdot ln\left(\frac{\left[Y_{ju}-f_{ju}(\xi)\right]^2}{number\ of\ independant\ event}\right) + 2.Number\ of\ estimated\ parameters \quad (12)$$

This criterion penalizes models with numerous parameters to estimate. Table 6 shows the values for each observable.

Table 6. AIC values for each observable and model.

	AIC				Number of parameters to estimate
	BL	**BHP**	**GVL**	**Tr**	
ER1	2529	2010	2151	36	6
LH1	2498	2008	2131	117	7
LH2	2500	2010	2133	118	8
NCLH1	2520	1993	2139	54	7
NCLH2	2508	2056	2161	38	8

Table 6 shows that NCLH1 and NCLH2 are the most reliable model by considering the AIC for all observables. Indeed, NCLH1 and NCLH2 models present a good compromise between the lowest AIC values for Tr and medium AIC values for BL, BHP and GVL.

For the sake of clarity, modeling results using NCLH1 model are displayed, and the others are in Supplementary Material (S2). Table 7 shows the value of the estimated parameters and the statistical values. The model can estimate the kinetic constants with low credible intervals. However, the estimation of adsorption constants is more challenging due to the difficulty to estimate such thermodynamic constants.

Table 7. Estimated values at T_{ref} = 398.15 K and statistical data for NCLH1.

	Units	Estimate	HPD	HPD%
$ln\left(k_1(T_{ref})\right)$	mol. kg_dry basis $RuC^{-1}.s^{-1}$	5.34	0.12	2.17
$ln\left(k_2(T_{ref})\right)$	s^{-1}	-10.19	0.03	0.28
$\frac{E_{a1}}{R \cdot T_{ref}}$	-	9.25	0.73	7.92
$\frac{E_{a2}}{R \cdot T_{ref}}$	-	8.09	0.59	7.27
$ln(K_H)$	$m^3.mol^{-1}$	-2.91	0.26	8.93
$ln(K_{BL^{\wedge}})$	$m^3.mol^{-1}$	0.011	-	
$ln(K_{BHP^{\wedge}})$	$m^3.mol^{-1}$	7.961	-	

Table 8. Normalized parameter covariance matrix for NCLH1.

	$ln\left(k_1(T_{ref})\right)$	$ln\left(k_2(T_{ref})\right)$	$\frac{E_{a1}}{R \cdot T_{ref}}$	$\frac{E_{a2}}{R \cdot T_{ref}}$	$ln(K_H)$
$ln\left(k_1(T_{ref})\right)$	1				
$ln\left(k_2(T_{ref})\right)$	0.07	1			
$\frac{E_{a1}}{R \cdot T_{ref}}$	-0.163	-0.047	1		
$\frac{E_{a2}}{R \cdot T_{ref}}$	-0.086	-0.671	-0.059	1	
$ln(K_H)$	-0.981	-0.071	0.123	0.081	1

Correlation between the majority of estimated parameters are lower than 0.90 in absolute value, thus one can consider that the estimated parameters are not correlated [108]. This absence of correlation shows that the parameters are well identified. The parameter $ln\left(k_1(T_{ref})\right)$ and $ln(K_H)$ are strongly correlated, due to the difficulty to correctly track the hydrogenation rate.

Figs 4-6 show the fit of the model to experimental data in different thermal modes for NCLH1 model. Generally, the model fits well the experimental data in these modes as it is confirmed with the parity plot (Fig. 7). In isothermal mode, experimental temperatures were not considered in the objective function, because the reaction temperature is stable along the reaction course. For adiabatic and isoperibolic experiments, we measured concentrations at the beginning and at the end of the reaction.

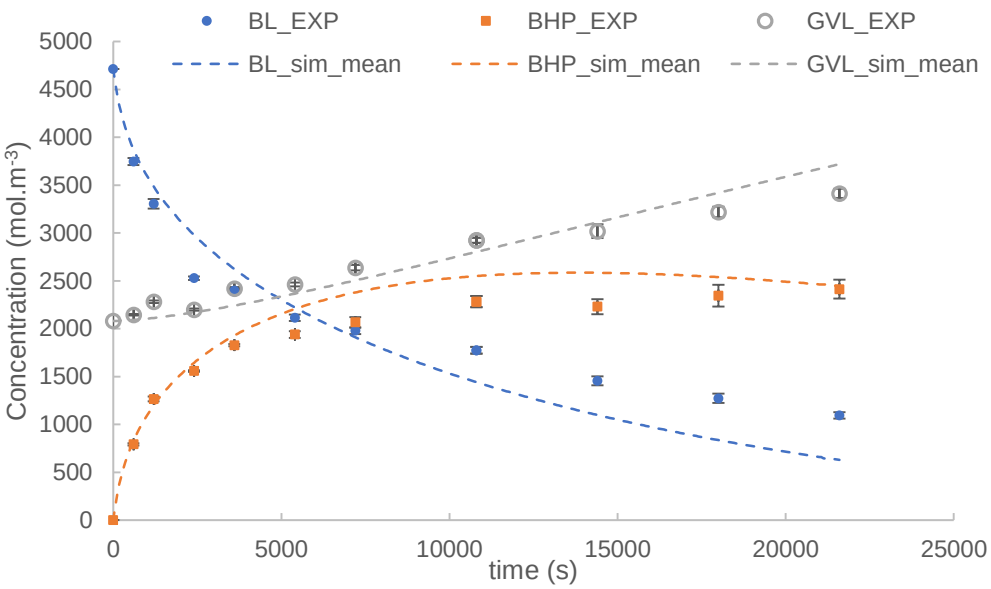

289

290 Fig. 4. Fit of the NCLH1 model to isothermal experimental data for Run 1.

291

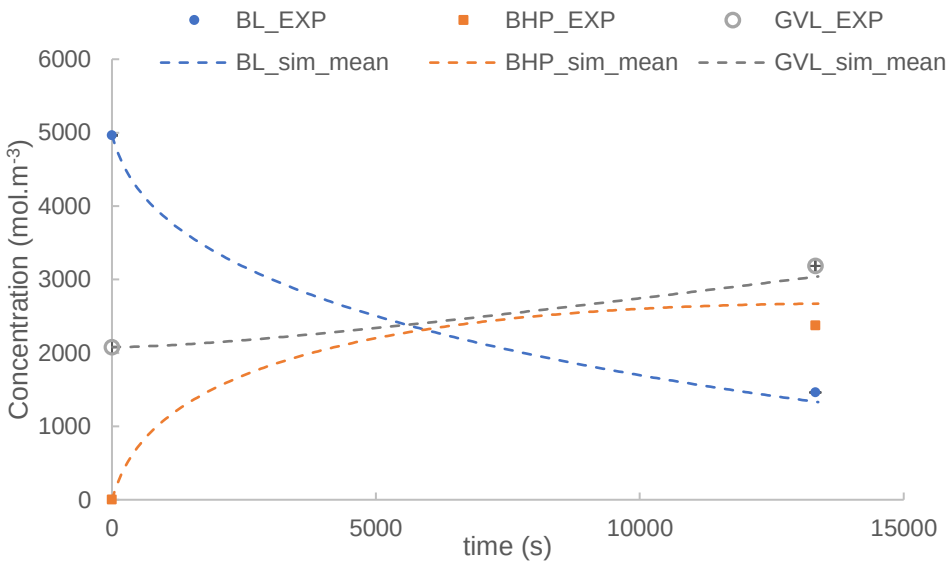

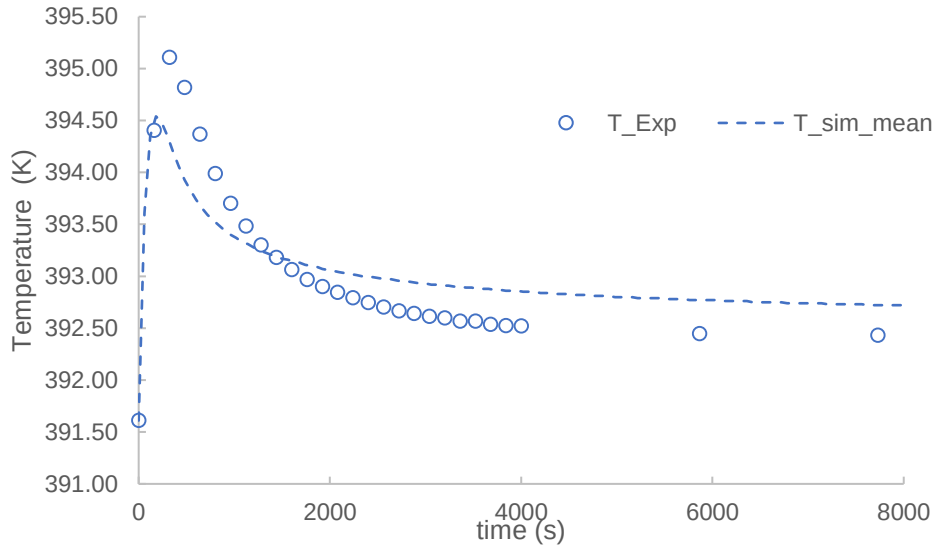

Fig. 5. Fit of the NCLH1 model to isoperibolic experimental data for Run 2.

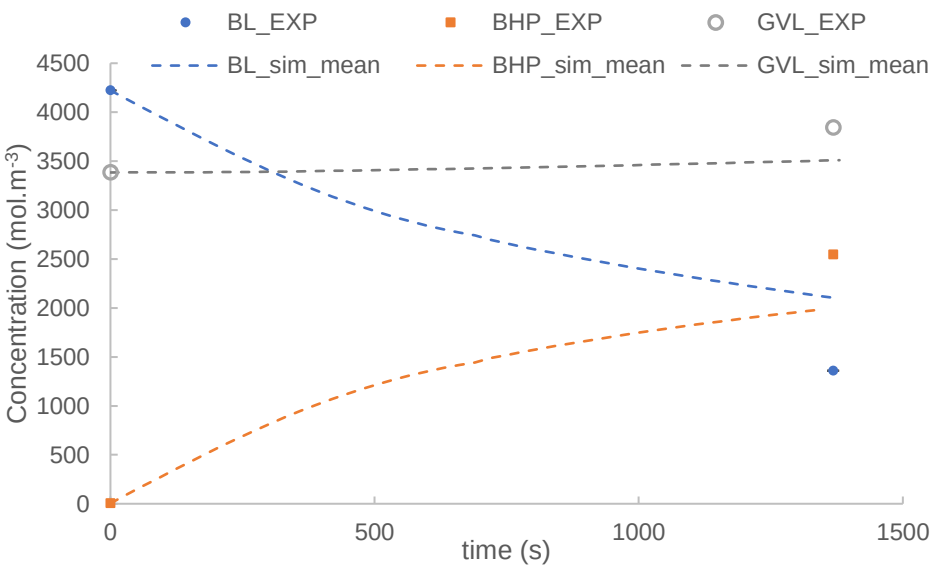

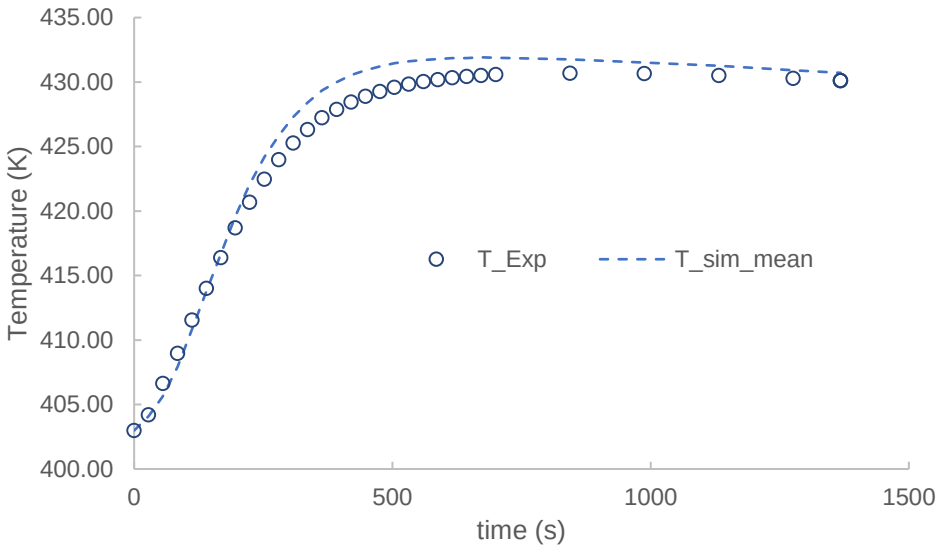

Fig. 6. Fit of the NCLH2 model to adiabatic experimental data for Run 6.

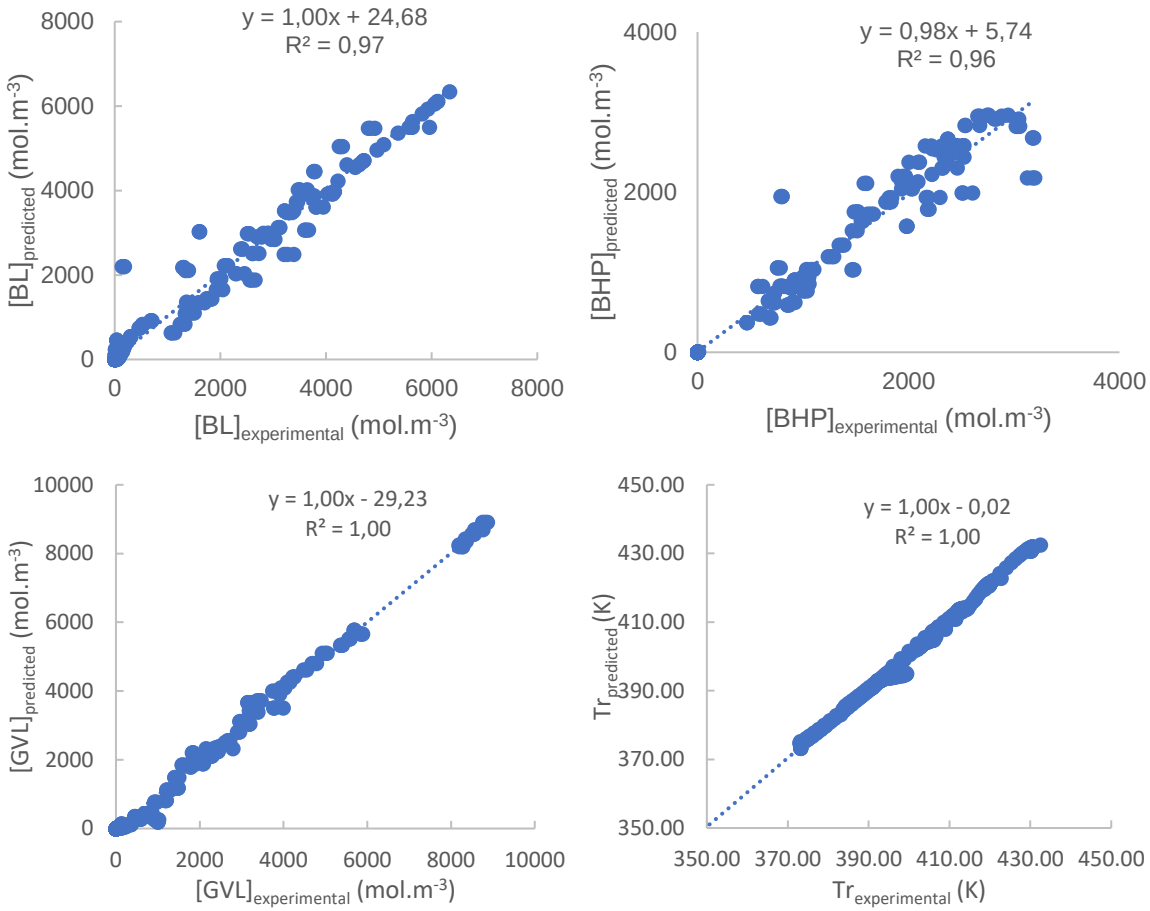

Fig. 7. Parity plots from regression stage (model NCLH1)

3.5.2. Validation stage

A holdout validation method was used. The estimated kinetic and thermodynamic constants obtained from the regression stage were used to predict the kinetic profile by using initial experimental conditions from Table 3. Fig. 8 show parity plots for the validation experiments for NCLH1, showing the good prediction capacity of NCLH1. NCLH1 can correctly predict BL and GVL concentrations, as well as reaction temperature. This model is less accurate for BHP concentration.

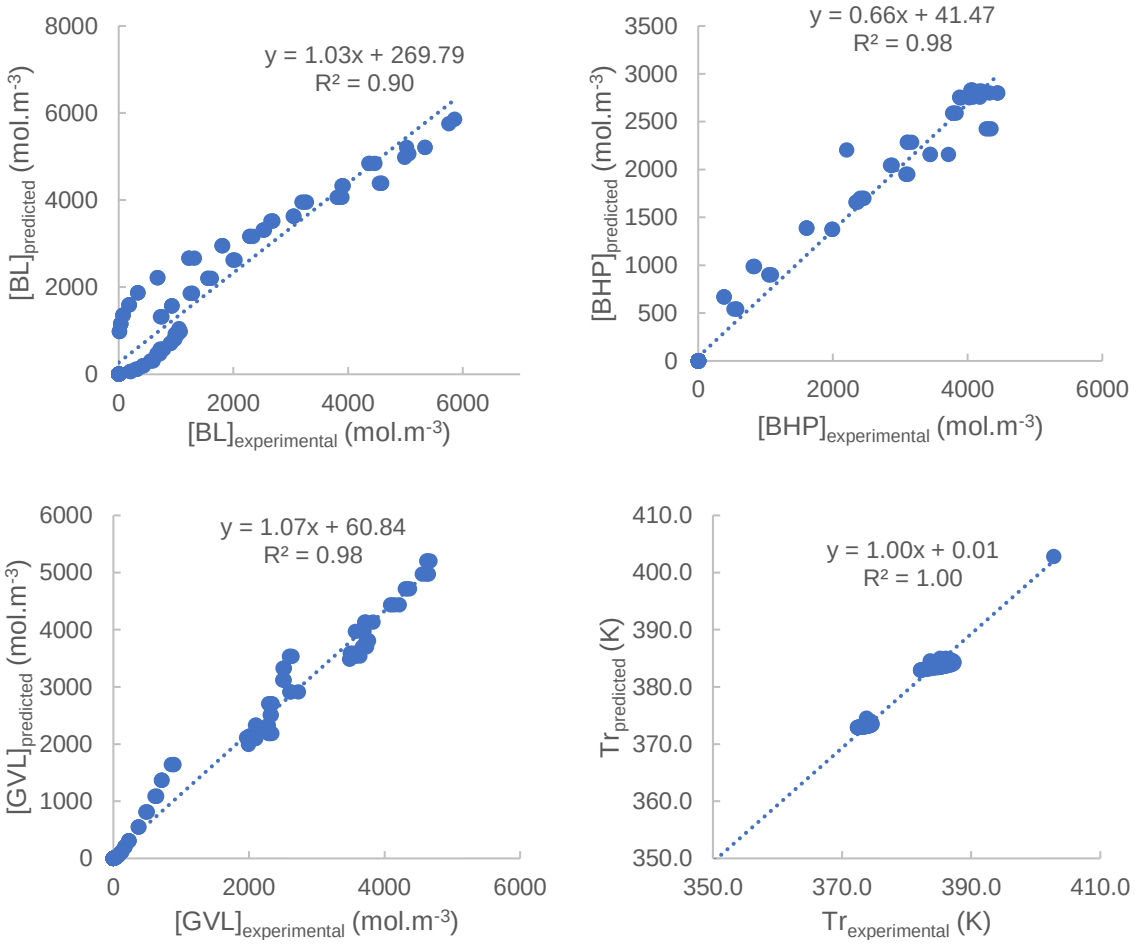

Fig. 8. Parity plots from validation stage (model NCLH1)

4. Conclusions

There is a need to develop reliable and robust kinetic models to scaleup, optimize process production, energy consumption and production, cost production and for thermal risk assessment. Traditionally, these types of kinetic models are developed in isothermal conditions without considering the energy balance. Thus, such models are limited for energy optimization or thermal risk assessment.

In this work, we developed and assessed 5 kinetic models in different thermal modes, i.e., isothermal, adiabatic and isoperibolic one. We applied this approach for the production of γ-valerolactone from the hydrogenation of butyl levulinate. To the best of the authors' knowledge, it is the first time that kinetic model are done in different thermal modes. Such models can provide crucial information in process optimization, scaleup, energy recovery for pinch analysis and thermal risk assessment.

Kinetic experiments were performed by using high concentrated solution of BL in the RC1 calorimeter using three thermal modes (isothermal, isoperibolic and adiabatic). For the regression stage, we varied the initial temperature from 383 to 430 K, catalyst loading from 6.5 to 13.5 kg/m^3 and hydrogen pressure from 15 to 35 bar. We were able to estimate kinetic constants for 5 kinetic models: Eley-Rideal with no adsorption of hydrogen (ER1), Langmuir Hinshelwood with molecular adsorption of H_2 (LH1), Langmuir Hinshelwood with hydrogen dissociation (LH2), Non-competitive Langmuir Hinshelwood with no dissociation of hydrogen (NCLH1) and Non-competitive Langmuir Hinshelwood with hydrogen dissociation (NCLH2). From the AIC criterion, we found that NCLH1 and NCLH2 models were the most reliable model. A validation stage was done using a holdout method, and confirmed the reliability of NCLH1 model.

A continuation of this work could be the determination of these constants from quantum mechanics method.

Acknowledgments

This investigation was carried out in the framework of the ARBRE project (Risk Analysis to processes valorizing 2nd generation biomass and using Renewable energies). ARBRE is cofounded by European Union through the European Regional Development Fund (agreement n° 00130305) and by Normandy Region (agreement n° 21E05304), via the support of "pôle CTM (Continuum Terre-Mer) and EP2M (Énergies, Propulsion, Matière, Matériaux) de Normandie université". The authors thank the Ministry of High Education, Science and Technology of Dominican Republic (MESCYT).

For the analytical part, this work has been partially supported by University of Rouen Normandy, INSA Rouen Normandy, the Centre National de la Recherche Scientifique (CNRS), European Regional Development Fund (ERDF) N° HN0001343, Labex SynOrg (ANR-11-LABX-0029), Carnot Institute I2C, the graduate school for reasearch XL-Chem (ANR-18-EURE-0020 XL CHEM) and by Region Normandie. GC was financed by FEDER RIN Green Chem 2019NU01FOBC08 Number: 17P04374.

355 **References**

356 [1] Rapier R. Highlights From The BP Statistical Review Of World Energy 2021 2021.
357 https://sourcezon.com/articles/highlights-from-the-bp-statistical-review-of-world-energy-
358 2021?slug=highlights-from-the-bp-statistical-review-of-world-energy-2021&q= (accessed
359 February 5, 2023).

360 [2] Manikandan S, Vickram S, Sirohi R, Subbaiya R, Krishnan RY, Karmegam N, et al. Critical
361 review of biochemical pathways to transformation of waste and biomass into bioenergy.
362 Bioresour Technol 2023;372:128679. https://doi.org/10.1016/j.biortech.2023.128679.

363 [3] Amerit B, Ntayi JM, Ngoma M, Bashir H, Echegu S, Nantongo M. Commercialization of
364 biofuel products: A systematic literature review. Renew Energy Focus 2023;44:223–36.
365 https://doi.org/10.1016/j.ref.2022.12.008.

366 [4] Jiang Y, Li Z, Li Y, Chen L, Zhang H, Li H, et al. Recent advances in sustainable catalytic
367 production of 5-methyl-2-pyrrolidones from bio-derived levulinate. Fuel 2023;334:126629.
368 https://doi.org/10.1016/j.fuel.2022.126629.

369 [5] Ashokkumar V, Venkatkarthick R, Jayashree S, Chuetor S, Dharmaraj S, Kumar G, et al.
370 Recent advances in lignocellulosic biomass for biofuels and value-added bioproducts - A
371 critical review. Bioresour Technol 2022;344:960–8524.
372 https://doi.org/10.1016/j.biortech.2021.126195.

373 [6] Liu WJ, Yu HQ. Thermochemical Conversion of Lignocellulosic Biomass into Mass-
374 Producible Fuels: Emerging Technology Progress and Environmental Sustainability
375 Evaluation. ACS Environ Au 2022;2:98–114. https://doi.org/10.1021/acsenvironau.1c00025.

376 [7] Jamil F, Saleem M, Ali Qamar O, Khurram MS, Al-Muhtaseb AH, Inayat A, et al. State-of-the-
377 art catalysts for clean fuel (methyl esters) production—a comprehensive review. JPhys Energy
378 2023;5:014005. https://doi.org/10.1088/2515-7655/aca5b3.

379 [8] Tomei J, Helliwell R. Food versus fuel? Going beyond biofuels. Land Use Policy

2016;56:320–6. https://doi.org/10.1016/j.landusepol.2015.11.015.

[9] Alonso DM, Wettstein SG, Mellmer MA, Gurbuz EI, Dumesic JA. Integrated conversion of hemicellulose and cellulose from lignocellulosic biomass. Energy Environ Sci 2013;6:76–80. https://doi.org/10.1039/c2ee23617f.

[10] Li G, Liu W, Ye C, Li X, Si CL. Chemocatalytic Conversion of Cellulose into Key Platform Chemicals. Int J Polym Sci 2018;2018. https://doi.org/10.1155/2018/4723573.

[11] Guo K, Guan Q, Xu J, Tan W. Mechanism of Preparation of Platform Compounds from Lignocellulosic Biomass Liquefaction Catalyzed by Bronsted Acid: A Review. J Bioresour Bioprod 2019;4:202–13. https://doi.org/10.12162/jbb.v4i4.009.

[12] Di Menno Di Bucchianico D, Wang Y, Buvat JC, Pan Y, Casson Moreno V, Leveneur S. Production of levulinic acid and alkyl levulinates: A process insight. Green Chem 2022;24:614–46. https://doi.org/10.1039/d1gc02457d.

[13] Yan K, Yang Y, Chai J, Lu Y. Catalytic reactions of gamma-valerolactone: A platform to fuels and value-added chemicals. Appl Catal B Environ 2015;179:292–304. https://doi.org/10.1016/J.APCATB.2015.04.030.

[14] Kerkel F, Markiewicz M, Stolte S, Müller E, Kunz W. The green platform molecule gamma-valerolactone - ecotoxicity, biodegradability, solvent properties, and potential applications. Green Chem 2021;23:2962–76. https://doi.org/10.1039/d0gc04353b.

[15] Qu R, Junge K, Beller M. Hydrogenation of Carboxylic Acids, Esters, and Related Compounds over Heterogeneous Catalysts: A Step toward Sustainable and Carbon-Neutral Processes. Chem Rev 2022. https://doi.org/10.1021/acs.chemrev.2c00550.

[16] Di Menno Di Bucchianico D, Buvat JC, Mignot M, Casson Moreno V, Leveneur S. Role of solvent the production of butyl levulinate from fructose. Fuel 2022;318:123703. https://doi.org/10.1016/j.fuel.2022.123703.

[17] Liu C, Wei M, Wang J, Xu J, Jiang J, Wang K. Facile Directional Conversion of Cellulose and

Bamboo Meal Wastes over Low-Cost Sulfate and Polar Aprotic Solvent. ACS Sustain Chem Eng 2020;8:5776–86. https://doi.org/10.1021/acssuschemeng.0c01280.

[18] Wang S, Zhao Y, Lin H, Chen J, Zhu L, Luo Z. Conversion of C5 carbohydrates into furfural catalyzed by a Lewis acidic ionic liquid in renewable γ-valerolactone. Green Chem 2017;19:3869–79. https://doi.org/10.1039/c7gc01298e.

[19] Chew AK, Walker TW, Shen Z, Demir B, Witteman L, Euclide J, et al. Effect of Mixed-Solvent Environments on the Selectivity of Acid-Catalyzed Dehydration Reactions. ACS Catal 2020;10:1679–91. https://doi.org/10.1021/acscatal.9b03460.

[20] Kang D, Choi M, Kim D, Han J. Environmental Analysis of Catalytic Adipic Acid Production Strategies from Two Different Lignocellulosic Biomasses. ACS Sustain Chem Eng 2022. https://doi.org/10.1021/acssuschemeng.2c00070.

[21] Motagamwala AH, Won W, Maravelias CT, Dumesic JA. An engineered solvent system for sugar production from lignocellulosic biomass using biomass derived γ-valerolactone. Green Chem 2016;18:5756–63. https://doi.org/10.1039/c6gc02297a.

[22] Baco S, Klinksiek M, Ismail Bedawi Zakaria R, Antonia Garcia-Hernandez E, Mignot M, Legros J, et al. Solvent effect investigation on the acid-catalyzed esterification of levulinic acid by ethanol aided by a Linear Solvation Energy Relationship. Chem Eng Sci 2022;260:117928. https://doi.org/10.1016/j.ces.2022.117928.

[23] Pokorný V, Štejfa V, Fulem M, Červinka C, Růžička K. Vapor Pressures and Thermophysical Properties of Ethylene Carbonate, Propylene Carbonate, γ-Valerolactone, and γ-Butyrolactone. J Chem Eng Data 2017;62:4174–86. https://doi.org/10.1021/acs.jced.7b00578.

[24] Ariba H, Wang Y, Devouge-Boyer C, Stateva RP, Leveneur S. Physicochemical Properties for the Reaction Systems: Levulinic Acid, Its Esters, and γ-Valerolactone. J Chem Eng Data 2020;65:3008–20. https://doi.org/10.1021/acs.jced.9b00965.

[25] Horváth IT, Mehdi H, Fábos V, Boda L, Mika LT. γ-Valerolactone—a sustainable liquid for

energy and carbon-based chemicals. Green Chem 2008;10:238–24. https://doi.org/10.1039/b712863k.

[26] Raj T, Chandrasekhar K, Banu R, Yoon JJ, Kumar G, Kim SH. Synthesis of γ-valerolactone (GVL) and their applications for lignocellulosic deconstruction for sustainable green biorefineries. Fuel 2021;303:121333. https://doi.org/10.1016/j.fuel.2021.121333.

[27] Al-Naji M, Puértolas B, Kumru B, Cruz D, Bäumel M, Schmidt BVKJ, et al. Sustainable Continuous Flow Valorization of γ-Valerolactone with Trioxane to α-Methylene-γ-Valerolactone over Basic Beta Zeolites. ChemSusChem 2019;12:2628–36. https://doi.org/10.1002/cssc.201900418.

[28] Manzer LE. Catalytic synthesis of α-methylene-γ-valerolactone: a biomass-derived acrylic monomer. Appl Catal A Gen 2004;272:249–56. https://doi.org/10.1016/J.APCATA.2004.05.048.

[29] Choi M, Byun J, Park H, Jeong K, Kim SM, Han J. Economically-feasible "greener" transformation of gamma-valerolactone to nylon 6,6. Biomass and Bioenergy 2022;162:106503. https://doi.org/10.1016/J.BIOMBIOE.2022.106503.

[30] Hayes G, Laurel M, MacKinnon D, Zhao T, Houck HA, Becer CR. Polymers without Petrochemicals: Sustainable Routes to Conventional Monomers. Chem Rev 2022. https://doi.org/10.1021/acs.chemrev.2c00354.

[31] Alonso DM, Bond JQ, Dumesic JA. Catalytic conversion of biomass to biofuels. Green Chem 2010;12:1493–513. https://doi.org/10.1039/c004654j.

[32] Dutta S, Yu IKM, Tsang DCW, Ng YH, Ok YS, Sherwood J, et al. Green synthesis of gamma-valerolactone (GVL) through hydrogenation of biomass-derived levulinic acid using non-noble metal catalysts: A critical review. Chem Eng J 2019;372:992–1006. https://doi.org/10.1016/j.cej.2019.04.199.

[33] Making alternative fuels cheaper | MIT News | Massachusetts Institute of Technology n.d.

https://news.mit.edu/2013/making-alternative-fuels-cheaper-0617 (accessed February 5, 2023).

[34] Anagnostopoulou E, Lilas P, Diamantopoulou P, Fakas C, Krithinakis I, Patatsi E, et al. Hydrogenation of the pivotal biorefinery platform molecule levulinic acid into renewable fuel γ-valerolactone catalyzed by unprecedented highly active and stable ruthenium nanoparticles in aqueous media. Renew Energy 2022;192:35–45. https://doi.org/10.1016/j.renene.2022.04.081.

[35] Kasar GB, Date NS, Bhosale PN, Rode C V. Steering the Ester and γ-Valerolactone Selectivities in Levulinic Acid Hydrogenation. Energy and Fuels 2018;32:6887–900. https://doi.org/10.1021/acs.energyfuels.8b01263.

[36] Alonso DM, Wettstein SG, Dumesic JA. Gamma-valerolactone, a sustainable platform molecule derived from lignocellulosic biomass. Green Chem 2013;15:584–95. https://doi.org/10.1039/c3gc37065h.

[37] Yan K, Lafleur T, Wu X, Chai J, Wu G, Xie X. Cascade upgrading of γ-valerolactone to biofuels. Chem Commun 2015;51:6984–7. https://doi.org/10.1039/c5cc01463h.

[38] Ayodele OO, Dawodu FA, Yan D, Dong H, Xin J, Zhang S. Production of Bio-Based Gasoline by Noble-Metal-Catalyzed Hydrodeoxygenation of α-Angelica Lactone Derived Di/Trimers. ChemistrySelect 2017;2:4219–25. https://doi.org/10.1002/slct.201700451.

[39] Wang H, Wu Y, Guo S, Dong C, Ding M. γ-Valerolactone converting to butene via ring-opening and decarboxylation steps over amorphous SiO2-Al2O3 catalyst. Mol Catal 2020;497:111218. https://doi.org/10.1016/j.mcat.2020.111218.

[40] Wang H, Wu Y, Li Y, Peng J, Gu XK, Ding M. One-step synthesis of pentane fuel from γ-valerolactone with high selectivity over a Co/HZSM-5 bifunctional catalyst. Green Chem 2021;23:4780–9. https://doi.org/10.1039/d1gc01062j.

[41] Bond JQ, Alonso DM, Wang D, West RM, Dumesic JA. Integrated catalytic conversion of γ-valerolactone to liquid alkenes for transportation fuels. Science (80-) 2010;327:1110–4. https://doi.org/10.1126/science.1184362.

[42] Han J. Integrated process for simultaneous production of jet fuel range alkenes and N-methylformanilide using biomass-derived gamma-valerolactone. J Ind Eng Chem 2017;48:173–9. https://doi.org/10.1016/j.jiec.2016.12.036.

[43] He J, Lin L, Liu M, Miao C, Wu Z, Chen R, et al. A durable Ni/La-Y catalyst for efficient hydrogenation of γ-valerolactone into pentanoic biofuels. J Energy Chem 2022;70:347–55. https://doi.org/10.1016/j.jechem.2022.02.011.

[44] Casson Moreno V, Garbetti AL, Leveneur S, Antonioni G. A consequences-based approach for the selection of relevant accident scenarios in emerging technologies. Saf Sci 2019;112:142–51. https://doi.org/10.1016/j.ssci.2018.10.024.

[45] Wang Y, Vernières-Hassimi L, Casson-Moreno V, Hébert JP, Leveneur S. Thermal Risk Assessment of Levulinic Acid Hydrogenation to γ-Valerolactone. Org Process Res Dev 2018;22:1092–100. https://doi.org/10.1021/acs.oprd.8b00122.

[46] Wang Y, Plazl I, Vernières-Hassimi L, Leveneur S. From calorimetry to thermal risk assessment: γ-Valerolactone production from the hydrogenation of alkyl levulinates. Process Saf Environ Prot 2020;144:32–41. https://doi.org/10.1016/j.psep.2020.07.017.

[47] Karanwal N, Kurniawan RG, Park J, Verma D, Oh S, Kim SM, et al. One-pot, cascade conversion of cellulose to γ-valerolactone over a multifunctional Ru–Cu/zeolite-Y catalyst in supercritical methanol. Appl Catal B Environ 2022;314:121466. https://doi.org/10.1016/j.apcatb.2022.121466.

[48] Siddiqui N, Pendem C, Goyal R, Khatun R, Khan TS, Samanta C, et al. Study of γ-valerolactone production from hydrogenation of levulinic acid over nanostructured Pt-hydrotalcite catalysts at low temperature. Fuel 2022;323:124272. https://doi.org/10.1016/j.fuel.2022.124272.

[49] Mehdi H, Fábos V, Tuba R, Bodor A, Mika LT, Horváth IT. Integration of homogeneous and heterogeneous catalytic processes for a multi-step conversion of biomass: From sucrose to

levulinic acid, γ-valerolactone, 1,4-pentanediol, 2-methyl-tetrahydrofuran, and alkanes. Top. Catal., vol. 48, Springer; 2008, p. 49–54. https://doi.org/10.1007/s11244-008-9047-6.

[50] Luo W, Deka U, Beale AM, Van Eck ERH, Bruijnincx PCA, Weckhuysen BM. Ruthenium-catalyzed hydrogenation of levulinic acid: Influence of the support and solvent on catalyst selectivity and stability. J Catal 2013;301:175–86. https://doi.org/10.1016/j.jcat.2013.02.003.

[51] Hengne AM, Rode C V. Cu–ZrO2 nanocomposite catalyst for selective hydrogenation of levulinic acid and its ester to γ-valerolactone. Green Chem 2012;14:1064–72. https://doi.org/10.1039/c2gc16558a.

[52] Piskun AS, van de Bovenkamp HH, Rasrendra CB, Winkelman JGM, Heeres HJ. Kinetic modeling of levulinic acid hydrogenation to γ-valerolactone in water using a carbon supported Ru catalyst. Appl Catal A Gen 2016;525:158–67. https://doi.org/10.1016/j.apcata.2016.06.033.

[53] Capecci S, Wang Y, Delgado J, Casson Moreno V, Mignot M, Grénman H, et al. Bayesian Statistics to Elucidate the Kinetics of γ-Valerolactone from n-Butyl Levulinate Hydrogenation over Ru/C. Ind Eng Chem Res 2021;60:11725–36. https://doi.org/10.1021/acs.iecr.1c02107.

[54] Capecci S, Wang Y, Casson Moreno V, Held C, Leveneur S. Solvent effect on the kinetics of the hydrogenation of n-butyl levulinate to γ-valerolactone. Chem Eng Sci 2021;231:116315. https://doi.org/10.1016/j.ces.2020.116315.

[55] Xu H, Hu D, Zhang M, Wang Y, Zhao Z, Jiang Z, et al. Bimetallic NiCu Alloy Catalysts for Hydrogenation of Levulinic Acid. ACS Appl Nano Mater 2021;4:3989–97. https://doi.org/10.1021/acsanm.1c00339.

[56] Al-Shaal MG, Wright WRH, Palkovits R. Exploring the ruthenium catalysed synthesis of γ-valerolactone in alcohols and utilisation of mild solvent-free reaction conditions. Green Chem 2012;14:1260–3. https://doi.org/10.1039/c2gc16631c.

[57] Wang Y, Cipolletta M, Vernières-Hassimi L, Casson-Moreno V, Leveneur S. Application of the concept of Linear Free Energy Relationships to the hydrogenation of levulinic acid and its

corresponding esters. Chem Eng J 2019;374:822–31. https://doi.org/10.1016/j.cej.2019.05.218.

[58] Li C, Xu G, Zhai Y, Liu X, Ma Y, Zhang Y. Hydrogenation of biomass-derived ethyl levulinate into Γ-valerolactone by activated carbon supported bimetallic Ni and Fe catalysts. Fuel 2017;203:23–31. https://doi.org/10.1016/j.fuel.2017.04.082.

[59] Yan K, Chen A. Selective hydrogenation of furfural and levulinic acid to biofuels on the ecofriendly Cu–Fe catalyst. Fuel 2014;115:101–8. https://doi.org/10.1016/J.FUEL.2013.06.042.

[60] Li Z, Hao H, Lu J, Wu C, Gao R, Li J, et al. Role of the Cu-ZrO2 interface in the hydrogenation of levulinic acid to γ-valerolactone. J Energy Chem 2021;61:446–58. https://doi.org/10.1016/j.jechem.2021.01.046.

[61] Fang S, Cui Z, Zhu Y, Wang C, Bai J, Zhang X, et al. In situ synthesis of biomass-derived Ni/C catalyst by self-reduction for the hydrogenation of levulinic acid to Γ-valerolactone. J Energy Chem 2019;37:204–14. https://doi.org/10.1016/j.jechem.2019.03.021.

[62] Orlowski I, Douthwaite M, Iqbal S, Hayward JS, Davies TE, Bartley JK, et al. The hydrogenation of levulinic acid to Γ-valerolactone over Cu–ZrO2 catalysts prepared by a pH-gradient methodology. J Energy Chem 2019;36:15–24. https://doi.org/10.1016/j.jechem.2019.01.015.

[63] Shen Q, Zhang Y, Zhang Y, Tan S, Chen J. Transformations of biomass-based levulinate ester into Γ-valerolactone and pyrrolidones using carbon nanotubes-grafted N-heterocyclic carbene ruthenium complexes. J Energy Chem 2019;39:29–38. https://doi.org/10.1016/j.jechem.2019.01.007.

[64] Delgado J, Vasquez Salcedo WN, Bronzetti G, Casson Moreno V, Mignot M, Legros J, et al. Kinetic model assessment for the synthesis of γ-valerolactone from n-butyl levulinate and levulinic acid hydrogenation over the synergy effect of dual catalysts Ru/C and Amberlite IR-120. Chem Eng J 2022;430:133053. https://doi.org/10.1016/j.cej.2021.133053.

[65] Shimizu KI, Kanno S, Kon K. Hydrogenation of levulinic acid to γ-valerolactone by Ni and MoO x co-loaded carbon catalysts. Green Chem 2014;16:3899–903. https://doi.org/10.1039/c4gc00735b.

[66] Hengne AM, Malawadkar A V., Biradar NS, Rode C V. Surface synergism of an Ag-Ni/ZrO2 nanocomposite for the catalytic transfer hydrogenation of bio-derived platform molecules. RSC Adv 2014;4:9730–6. https://doi.org/10.1039/c3ra46495d.

[67] Heeres H, Handana R, Chunai D, Borromeus Rasrendra C, Girisuta B, Jan Heeres H. Combined dehydration/(transfer)-hydrogenation of C6-sugars (D-glucose and D-fructose) to γ-valerolactone using ruthenium catalysts. Green Chem 2009;11:1247–55. https://doi.org/10.1039/b904693c.

[68] Fellay C, Dyson PJ, Laurenczy G. A viable hydrogen-storage system based on selective formic acid decomposition with a ruthenium catalyst. Angew Chemie - Int Ed 2008;47:3966–8. https://doi.org/10.1002/anie.200800320.

[69] Fábos V, Mika LT, Horváth IT. Selective conversion of levulinic and formic acids to γ-valerolactone with the shvo catalyst. Organometallics 2014;33:181–7. https://doi.org/10.1021/om400938h.

[70] Deng L, Zhao Y, Li J, Fu Y, Liao B, Guo QX. Conversion of levulinic acid and formic acid into γ-valerolactone over heterogeneous catalysts. ChemSusChem 2010;3:1172–5. https://doi.org/10.1002/cssc.201000163.

[71] Deng L, Li J, Lai DM, Fu Y, Guo QX. Catalytic conversion of biomass-derived carbohydrates into γ-valerolactone without using an external h2 supply. Angew Chemie - Int Ed 2009;48:6529–32. https://doi.org/10.1002/anie.200902281.

[72] Ruppert AM, Jędrzejczyk M, Sneka-Płatek O, Keller N, Dumon AS, Michel C, et al. Ru catalysts for levulinic acid hydrogenation with formic acid as a hydrogen source. Green Chem 2016;18:2014–28. https://doi.org/10.1039/c5gc02200b.

[73] Yuan J, Li SS, Yu L, Liu YM, Cao Y, He HY, et al. Copper-based catalysts for the efficient conversion of carbohydrate biomass into γ-valerolactone in the absence of externally added hydrogen. Energy Environ Sci 2013;6:3308–13. https://doi.org/10.1039/c3ee40857d.

[74] Son PA, Nishimura S, Ebitani K. Production of γ-valerolactone from biomass-derived compounds using formic acid as a hydrogen source over supported metal catalysts in water solvent. RSC Adv 2014;4:10525–30. https://doi.org/10.1039/c3ra47580h.

[75] Li H, Fang Z, Yang S. Direct catalytic transformation of biomass derivatives into biofuel component γ-valerolactone with magnetic nickel-zirconium nanoparticles. Chempluschem 2016;81:135–42. https://doi.org/10.1002/cplu.201500492.

[76] Chia M, Dumesic JA. Liquid-phase catalytic transfer hydrogenation and cyclization of levulinic acid and its esters to γ-valerolactone over metal oxide catalysts. Chem Commun 2011;47:12233–5. https://doi.org/10.1039/c1cc14748j.

[77] Li H, Fang Z, Yang S. Direct Conversion of Sugars and Ethyl Levulinate into γ-Valerolactone with Superparamagnetic Acid-Base Bifunctional ZrFeOx Nanocatalysts. ACS Sustain Chem Eng 2016;4:236–46. https://doi.org/10.1021/acssuschemeng.5b01480.

[78] Ju Z, Feng S, Ren L, Lei T, Cheng H, Yu M, et al. Probing the mechanism of the conversion of methyl levulinate into γ-valerolactone catalyzed by Al(OiPr)3in an alcohol solvent: A DFT study. RSC Adv 2022;12:2788–97. https://doi.org/10.1039/d1ra08429a.

[79] Ortuño MA, Rellán-Piñeiro M, Luque R. Computational Mechanism of Methyl Levulinate Conversion to γ-Valerolactone on UiO-66 Metal Organic Frameworks. ACS Sustain Chem Eng 2022;10:3567–73. https://doi.org/10.1021/acssuschemeng.1c08021.

[80] Chen X, Zhao T, Zhang X, Zhang Y, Yu H, Lyu Q, et al. Synthesis of ternary magnetic nanoparticles for enhanced catalytic conversion of biomass-derived methyl levulinate into γ-valerolactone. J Energy Chem 2021;63:430–41. https://doi.org/10.1016/j.jechem.2021.07.013.

[81] Zhang C, Huo Z, Ren D, Song Z, Liu Y, Jin F, et al. Catalytic transfer hydrogenation of

levulinate ester into γ-valerolactone over ternary Cu/ZnO/Al 2 O 3 catalyst. J Energy Chem 2019;32:189–97. https://doi.org/10.1016/j.jechem.2018.08.001.

[82] Wu J, Zhu Y, Liao P, Xu T, Lu L, Zhang X, et al. Sustainable metal-lignosulfonate catalyst for efficient catalytic transfer hydrogenation of levulinic acid to γ-valerolactone. Appl Catal A Gen 2022;635:118556. https://doi.org/10.1016/j.apcata.2022.118556.

[83] Protsenko II, Nikoshvili LZ, Matveeva VG, Sulman EM. Kinetic Modelling of Levulinic Acid Hydrogenation Over Ru-Containing Polymeric Catalyst. Top Catal 2020;63:243–53. https://doi.org/10.1007/s11244-020-01223-0.

[84] Huang X, Liu K, Vrijburg WL, Ouyang X, Iulian Dugulan A, Liu Y, et al. Hydrogenation of levulinic acid to γ-valerolactone over Fe-Re/TiO2 catalysts. Appl Catal B Environ 2020;278:119314. https://doi.org/10.1016/j.apcatb.2020.119314.

[85] Chalid M, Broekhuis AA, Heeres HJ. Experimental and kinetic modeling studies on the biphasic hydrogenation of levulinic acid to γ-valerolactone using a homogeneous water-soluble Ru-(TPPTS) catalyst. J Mol Catal A Chem 2011;341:14–21. https://doi.org/10.1016/j.molcata.2011.04.004.

[86] Abdelrahman OA, Heyden A, Bond JQ. Analysis of kinetics and reaction pathways in the aqueous-phase hydrogenation of levulinic acid to form γ-Valerolactone over Ru/C. ACS Catal 2014;4:1171–81. https://doi.org/10.1021/cs401177p.

[87] Molleti J, Tiwari MS, Yadav GD. Novel synthesis of Ru/OMS catalyst by solvent-free method: Selective hydrogenation of levulinic acid to Γ-valerolactone in aqueous medium and kinetic modelling. Chem Eng J 2018;334:2488–99. https://doi.org/10.1016/j.cej.2017.11.125.

[88] Leveneur S, Pinchard M, Rimbault A, Safdari Shadloo M, Meyer T. Parameters affecting thermal risk through a kinetic model under adiabatic condition: Application to liquid-liquid reaction system. Thermochim Acta 2018;666:10–7. https://doi.org/10.1016/j.tca.2018.05.024.

[89] Cao CR, Liu SH. Thermal hazard characteristic evaluation of two low-temperature-reactive azo

compounds under adiabatic process conditions. Process Saf Environ Prot 2019;130:231–7. https://doi.org/10.1016/j.psep.2019.08.020.

[90] Bhattacharya A. A general kinetic model framework for the interpretation of adiabatic calorimeter rate data. Chem Eng J 2005;110:67–78. https://doi.org/10.1016/j.cej.2005.05.003.

[91] Stoessel F. Thermal Safety of Chemical Processes: Risk Assessment and Process Design. Wiley-VCH; 2008. https://doi.org/10.1002/9783527621606.

[92] Zheng JL, Wärnå J, Salmi T, Burel F, Taouk B, Leveneur S. Kinetic modeling strategy for an exothermic multiphase reactor system: Application to vegetable oils epoxidation using Prileschajew method. AIChE J 2016;62:726–41. https://doi.org/10.1002/aic.15037.

[93] Xie Q, Zhang Z, Zhang L, Xie Y, Liu W, Chen H. Thermal decomposition behavior and kinetics for nitrolysis solution from the nitration of hexamethylenetetramine. React Kinet Mech Catal 2019;128:645–62. https://doi.org/10.1007/s11144-019-01658-x.

[94] Andreozzi R, Canterino M, Caprio V, Di Somma I, Sanchirico R. Batch salicylic acid nitration by nitric acid/acetic acid mixture under isothermal, isoperibolic and adiabatic conditions. J Hazard Mater 2006;138:452–8. https://doi.org/10.1016/j.jhazmat.2006.05.104.

[95] Alamgir Ahmad K, Haider Siddiqui M, Pant KK, Nigam KDP, Shetti NP, Aminabhavi TM, et al. A critical review on suitability and catalytic production of butyl levulinate as a blending molecule for green diesel. Chem Eng J 2022;447:137550. https://doi.org/10.1016/j.cej.2022.137550.

[96] Delgado J, Vásquez Salcedo WN, Devouge-Boyer C, Hebert JP, Legros J, Renou B, et al. Reaction enthalpies for the hydrogenation of alkyl levulinates and levulinic acid on Ru/C–influence of experimental conditions and alkyl chain length. Process Saf Environ Prot 2023;171:289–98. https://doi.org/10.1016/j.psep.2023.01.025.

[97] Zheng JL, Wärnå J, Salmi T, Burel F, Taouk B, Leveneur S. Kinetic modeling strategy for an exothermic multiphase reactor system: Application to vegetable oils epoxidation using

Prileschajew method. AIChE J 2016;62:726–41. https://doi.org/10.1002/aic.15037.

[98] Lavanchy F. Development of reaction calorimetry... - Google Scholar. n.d.

[99] Nasrifar K. Comparative study of eleven equations of state in predicting the thermodynamic properties of hydrogen. Int J Hydrogen Energy 2010;35:3802–11. https://doi.org/10.1016/j.ijhydene.2010.01.032.

[100] Stewart WE, Caracotsios M. Computer-Aided Modeling of Reactive Systems. First. New Jersey: 2008. https://doi.org/10.1002/9780470282038.

[101] Stewart WE, Caracotsios M, Sørensen JP. Parameter estimation from multiresponse data. AIChE J 1992. https://doi.org/10.1002/aic.690380502.

[102] Kopyscinski J, Choi J, Hill JM. Comprehensive kinetic study for pyridine hydrodenitrogenation on (Ni)WP/SiO2 catalysts. Appl Catal A Gen 2012;445–446:50–60. https://doi.org/10.1016/j.apcata.2012.08.027.

[103] Van Boekel MAJS. Statistical aspects of kinetic modeling for food science problems. J Food Sci 1996;61:477–86. https://doi.org/10.1111/j.1365-2621.1996.tb13138.x.

[104] Caracotsios M, Stewart WE. Sensitivity analysis of initial value problems with mixed odes and algebraic equations. Comput Chem Eng 1985;9:359–65. https://doi.org/10.1016/0098-1354(85)85014-6.

[105] Capecci S, Wang Y, Delgado J, Casson Moreno V, Mignot M, Grénman H, et al. Bayesian Statistics to Elucidate the Kinetics of γ-Valerolactone from n-Butyl Levulinate Hydrogenation over Ru/C. Ind Eng Chem Res 2021;60:11725–36. https://doi.org/10.1021/ACS.IECR.1C02107/ASSET/IMAGES/LARGE/IE1C02107_0008.JPEG.

[106] Ariba H, Wang Y, Devouge-Boyer C, Stateva RP, Leveneur S. Physicochemical Properties for the Reaction Systems: Levulinic Acid, Its Esters, and γ-Valerolactone. J Chem Eng Data 2020;65:3008–20. https://doi.org/10.1021/acs.jced.9b00965.

[107] Lu X, Wang Y, Estel L, Kumar N, Grénman H, Leveneur S. Evolution of specific heat capacity with temperature for typical supports used for heterogeneous catalysts. Processes 2020;8:911. https://doi.org/10.3390/PR8080911.

[108] Toch K, Thybaut JW, Marin GB. A systematic methodology for kinetic modeling of chemical reactions applied to n-hexane hydroisomerization. AIChE J 2015;61:880–92. https://doi.org/10.1002/aic.14680.